The impact of moisture and temperature on the laminated rhombic hyperbolic paraboloid

**Abhay Chaubey[1], Ajay Kumar[2],
Małgorzata Grzegorczyk-Frańczak[3], Małgorzata Szafraniec[4]**

[1] *Department of Civil Engineering; Koneru Lakshmaiah Education Foundation; Vaddeswaram 522502, India;
abhaychaubey26@gmail.com; ORCID: 0000-0003-4607-9765*

[2] *Department of Civil Engineering; National Institute of Technology Patna; Patna-800005, India;
sajaydce@gmail.com; ORCID: 0000-0003-0083-9052*

[3] *Faculty of Civil Engineering and Architecture; Lublin University of Technology;
Nadbystrzycka 40, 20-618 Lublin, Poland;
m.grzegorczyk@pollub.pl; ORCID: 0000-0002-6119-2902*

[4] *Faculty of Civil Engineering and Architecture; Lublin University of Technology;
Nadbystrzycka 40, 20-618 Lublin, Poland;
m.szafraniec@pollub.pl; ORCID: 0000-0002-5862-9456*

Abstract: The current work presents a hygrothermal analysis of laminated composite rhombic hyperbolic paraboloids. The cubic variation in displacement field together with cross curvature effects of the shell were used to solve the hygrothermal problem. Because of the parabolic variation of the transverse shear deformation, the shear correction factor was not necessary in this paper. In the mathematical model, the zero conditions of the transverse shear stress at the bottom and top of the shell were applied. The nine-noded curved isoparametric element with seven unknowns in each node was used to implement the present realistic mathematical model. The implementation of the finite element C^0 (FE) of the present mathematical model was coded and performed in FORTRAN. The skew hyperbolic paraboloid on which the hygrothermal analysis was conducted had various temperatures, ply orientation, curvatures, moisture concentration, boundary conditions and thickness ratio. The paper shows that with the increase of the skew angle, the non-dimensional deflection decreases, and with the increase of moisture concentration, hygrothermal load and curvature ratio, the deflection increases. The results of the model presented in the paper were compared with other results published in the literature and were found to be consistent with them.

Keywords: temperature; moisture concentration; laminated; skew angle; ply orientation

1. Introduction

Laminated composite structures are gaining more and more attention today due to their improved properties, such as high strength-to-weight ratio, resistance to oxidation corrosion, high strength-to-rigidity ratio and improved toughness. Due to their advantages such as structural lightness and rigidity, laminated composite hyperbolic paraboloids are used in various industries. However, laminated structures are often exposed to moisture

loads and unfavourable temperatures during their service lifespan. Due to their porosity, building materials often contain water in their structure, which contributes to the reduction of their load capacity and thermal properties [1-3]. Temperature and moisture cause stress and deformation of laminated composite structures, which leads to their destruction. This is why it is so important to study laminated composite hyperbolic paraboloids subjected to hygrothermal load.

Pipes et al. [4] examined the hygrothermal response of the laminated composite plate. The classical diffusion equation was used in their study to describe the diffusion of moisture. Their results, though, were limited to thin geometry. The paper [5] presents the results of thermal stress and deformation tests on antisymmetric cross-ply and angle-ply laminates. The effect of moisture and temperature on the cylindrical composite shell was studied by Lee and Yen [6] using the FE method. The paper [7] develops and presents equations for the laminated composite plates which take into account the influence of expansive stress caused by moisture and temperature. To conduct the hygrothermal analysis of plate or shell, researchers have used various methods. In his work, Pell [8] examined the problem of thermal bending of thin anisotropic plates. The FE method with quadratic isoparametric element was used by Ram and Sinha [9] to determine the hygrothermal influence on the bending properties of laminates. Researchers in [10] developed a FE formula for an anisotropic composite panel subjected to thermal and mechanical loads. This study presents an exact closed-form solution for laminated composite plates subjected to sinusoidal loading. In [11], Lawrence and Doxsee applied the higher order theory to study the hygrothermal behaviour of shells. They used various shapes of shells as well as arbitrary temperature and moisture distributions. CLPT and the von Karman large deflection theory were used by Lee et al. [12] to investigate the effect of hygrothermal energy on the cylindrical bending of symmetric angle-ply laminates subjected to uniform transverse loading. Zenkour and Alghanmi [13] applied the sinusoidal shear deformation theory to investigate sinusoidal hygrothermal load of multilayer plates. The paper [14] presents experimental and numerical tests based on FSDT and applied in a dynamic analysis of laminated shallow shells in hygrothermal conditions. A single-layer model designed for thermal bending analysis of laminated cylindrical shells using FSDT was developed by Zenkour and Fares [15]. Singh and Chakrabarti [16] used an efficient HSDT to perform a hygrothermal analysis of laminates. Zenkour [17] applied a unified shear deformation plate theory to study thermo-elastic behaviour of symmetric and anti-symmetric cross-ply laminates. As part of a unified formula, Brischetto [18] proposed an improved 2D model for the bending analysis of multilayer composite and sandwich plates subjected to mechanical and hygrothermal loading. Upadhyaya et al. [19] conducted a non-linear bending analysis of laminates exposed to hygrothermal and mechanical loads. In [20], a hygrothermal analysis of cylindrical shells was carried out using HSDT. Patela et al. [21] applied HSDT to present the dynamic and static behaviour of thick composite laminates in hygrothermal conditions. Ali et al. [22] On the basis of the new higher order displacement theory, Ali et al. [22] developed an accurate model for mechanical and thermal analysis of thick laminates. Bending analysis of multilayer plates subjected to thermomechanical loading was presented by Brischetto and Carrera [23]. In [24], closed-form thermomechanical solutions for the analysis of double curved laminated shells with the use of 2D HSDT theory were described. Tauchert [25] presented the test of reaction to thermal load. The paper discusses large post-bending deformation, buckling, vibration analysis and thermally induced bending. Khdeir et al. [26] demonstrated thermal analysis of cross-ply shallow shells with the use of a precise analytical solution. In their

work [27], Jin and Yao showed an effective, improved C^0-type global/local model (IGLM) for a bending analysis of thick cross-ply laminates in hygrothermal load conditions. In [28], a direct, iterative C^0 non-linear FE method is presented for a spherical shell panel and plate exposed to hygro-thermo-mechanical loading.

The literature study showed that there are no hygrothermal analysis results concerning laminated composite rhombic hyperbolic paraboloids. Therefore, this paper aims to investigate their hygrothermal behaviour. For this study, the authors have developed a C^0 FE model based on a nine-noded continuous curved isoparametric element.

2. Mathematical formulas

2.1. Strains and displacement fields

Fig. 1 shows a laminated composite shell with the reference plane at $z = 0$ and the curvature R_x and R_y longitudinally to the x and y axes.
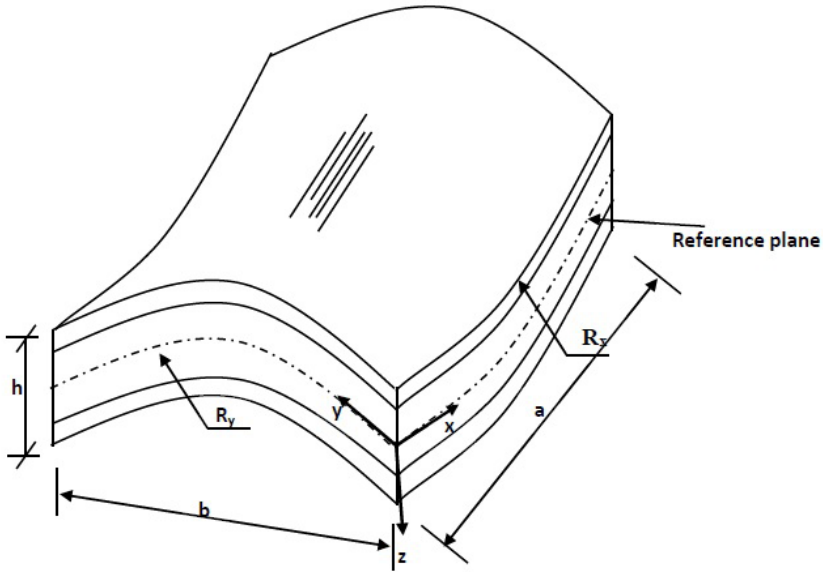

Fig. 1.   Laminated composite hyperbolic paraboloid shell, where *a* and *b* represent the sides of a hyperbolic paraboloid with a total thickness of h. Source: own study

Based on Reddy [29], the displacement fields are established and indicated as:

$$\{C\} = \{C_0\} + z\{\theta\} + z^2\{\xi\} + z^3\{\zeta\}$$ (1)

$$\{C\} = \{u, v, w\}^T, \{C_0\} = \{u_0, v_0, w_0\}^T, \theta = \{\theta_x, \theta_y, 0\}^T, \{\xi\} = \{\xi_x, \xi_y, 0\}^T \text{ and } \{\zeta\} = \{\zeta_x, \zeta_y, 0\}^T$$

where: ξ_x, ζ_x, ξ_y and ζ_y are higher-order terms of Taylor series expansion, υ is displacement, υ_0 – displacement of midpoints, $\theta_x(x, y)$ is the rotation of the normal along the y axis, u is displacement, υ_0 displacement of midpoints, and $\theta_y(x, y)$ is the rotation of the normal along x axis.

The developed displacement field shall be obtained by eliminating the transverse shear stress resultants at ± h/2 of the shell as follows:

$$\{C\} = \{C_0\} + z\left(1 - \frac{4z^2}{3h^2}\right)\{\theta\} - \frac{4z^3}{3h^2}\{\psi^*\} \quad \{C\} = \{C_0\} + z\left(1 - \frac{4z^2}{3h^2}\right)\{\theta\} - \frac{4z^3}{3h^2}\{\psi^*\} \text{ , where} \tag{2}$$

$$\{\psi^*\} = \{\psi_x^*, \psi_y^*, 0\} ,$$

$$\psi_x^* = \frac{\partial w}{\partial x}, \psi_y^* = \frac{\partial w}{\partial y}$$

{R} (the nodal degree of freedom) can be defined as:

$$\{R\} = \{u_0, v_0, w_0, \theta_x, \theta_y, \psi_x^*, \psi_y^*\} \tag{3}$$

Equation (4) shows a linear strain-displacement relationship, which is based on Sanders' approximation.

$$\varepsilon_{xx} = \frac{\partial u}{\partial x} + \frac{w}{R_x} , \ \varepsilon_{yy} = \frac{\partial v}{\partial y} + \frac{w}{R_y} , \ \gamma_{xy} = \frac{\partial v}{\partial x} + \frac{\partial u}{\partial y} + \frac{2w}{R_{xy}} \tag{4}$$

$$\gamma_{xz} = \frac{\partial u}{\partial z} + \frac{\partial w}{\partial x} - A_1 \frac{u}{R_x} - A_1 \frac{v}{R_{xy}} , \ \gamma_{yz} = \frac{\partial v}{\partial z} + \frac{\partial w}{\partial y} - A_1 \frac{v}{R_y} - A_1 \frac{u}{R_{xy}}$$

Substituting Equation (2) in Equation (5):

$$\begin{Bmatrix} \varepsilon_{xx} \\ \varepsilon_{yy} \\ \gamma_{xy} \end{Bmatrix} = \begin{Bmatrix} \varepsilon_{x0} \\ \varepsilon_{y0} \\ \varepsilon_{xy0} \end{Bmatrix} + z \begin{Bmatrix} K_x \\ K_y \\ K_{xy} \end{Bmatrix} - \frac{4z^3}{3h^2} \begin{Bmatrix} (K_x + K_x^*) \\ (K_y + K_y^*) \\ (K_{xy} + K_{xy}^*) \end{Bmatrix} \tag{5}$$

$$\begin{Bmatrix} \gamma_{xz} \\ \gamma_{yz} \end{Bmatrix} = \begin{Bmatrix} \phi_x \\ \phi_y \end{Bmatrix} + z \begin{Bmatrix} K_{xz} \\ K_{yz} \end{Bmatrix} - \frac{4z^2}{h^2} \begin{Bmatrix} K_{xz}^{**} \\ K_{yz}^{**} \end{Bmatrix} + \frac{4z^3}{3h^2} \begin{Bmatrix} K_{xz}^* \\ K_{yz}^* \end{Bmatrix} , \text{ where}$$

$$\{\varepsilon_{x0}, \varepsilon_{y0}, \varepsilon_{xy0}\} = \left\{ u_{0,x} + \frac{w}{R_x}, v_{0,y} + \frac{w}{R_y}, u_{0,y} + v_{0,x} + \frac{2w}{R_{xy}} \right\}$$

$$\{\phi_x, \phi_y\} = \left\{ w_{0,x} + \theta_x - A_1 \frac{u_0}{R_x} - A_1 \frac{v_0}{R_{xy}}, w_{0,y} + \theta_y - A_1 \frac{v_0}{R_y} - A_1 \frac{u_0}{R_{xy}} \right\}$$

$$\{K_x, K_y, K_{xy}, K_x^*, K_y^*, K_{xy}^*\} = \{\theta_{x,x}, \theta_{y,y}, \theta_{x,y} + \theta_{y,x}, \psi_{x,x}^*, \psi_{y,y}^*, \psi_{x,y}^* + \psi_{y,x}^*\}$$

$$\{K_{xz}, K_{yz}, K_{xz}^*, K_{yz}^*\} = \left\{ -A_1 \frac{\theta_x}{R_x} - A_1 \frac{\theta_y}{R_{xy}}, -A_1 \frac{\theta_y}{R_y} - A_1 \frac{\theta_x}{R_{xy}}, A_1 \frac{\theta_x}{R_x} + A_1 \frac{\theta_y}{R_{xy}}, A_1 \frac{\theta_y}{R_y} + A_1 \frac{\theta_x}{R_{xy}} \right\}$$

$$\{K_{xz}^{**}, K_{yz}^{**}\} = \{\theta_x + \psi_x^*, \theta_y + \psi_y^*\}$$

To shorten the analysis to Love's first approximation, the tracer coefficient (A1) is used.

2.2. Consecutive Equation

$$\begin{Bmatrix} \sigma_x \\ \sigma_y \\ \tau_{xy} \\ \tau_{yz} \\ \tau_{xz} \end{Bmatrix}_k = \begin{bmatrix} \overline{Q}_{11} & \overline{Q}_{12} & \overline{Q}_{16} & 0 & 0 \\ \overline{Q}_{12} & \overline{Q}_{22} & \overline{Q}_{26} & 0 & 0 \\ \overline{Q}_{16} & \overline{Q}_{26} & \overline{Q}_{66} & 0 & 0 \\ 0 & 0 & 0 & \overline{Q}_{44} & \overline{Q}_{45} \\ 0 & 0 & 0 & \overline{Q}_{45} & \overline{Q}_{55} \end{bmatrix}_k \begin{Bmatrix} \varepsilon_x - \alpha_x \Delta T - \beta_x \Delta C \\ \varepsilon_y - \alpha_y \Delta T - \beta_y \Delta C \\ \gamma_{xy} - \alpha_{xy} \Delta T - \beta_{xy} \Delta C \\ \gamma_{yz} \\ \gamma_{xz} \end{Bmatrix}_k, \tag{6}$$

where: $[\overline{Q}_{ij}]$ is transformed reduced stiffness matrix, β_x; β_y; β_{xy} – transformed contraction or swelling coefficients (moisture), α_x; α_y; α_{xy} – transformed thermal contraction or expansion coefficients (temperature), ΔC – moisture concentration change, ΔT – temperature change.

3. The formulation of finite elements

Fig. 2 shows a nine-noded isoparametric element used for the analysis in (7).

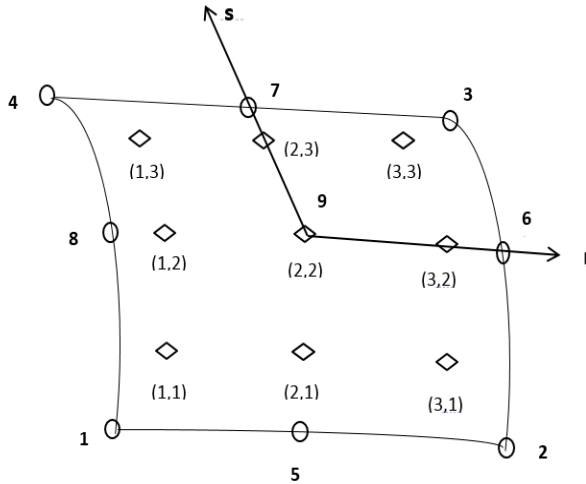

Fig. 2.   The curved isoparametric element with nine nodes (Gauss points and typical node numbering). Source: own study

$$\{w\} = [N]\{\delta\} \tag{7}$$

The equations (8) shown below can be used to find stress at any point.

$$\{\overline{\sigma}\} = [\overline{Q}]\{\overline{\varepsilon_n}\} \tag{8}$$

where: $\{\overline{\varepsilon_n}\} = \{\overline{\varepsilon} - \overline{\varepsilon_{th}} - \overline{\varepsilon_m}\}$.

The total strain ε_n is shown in the equation (9):

$$\{\overline{\varepsilon}\} = [H]\{\varepsilon\}, \tag{9}$$

where: ε is strain from mechanical loads, ε_m – strain from moisture, ε_{th} – strain from thermal loads.

$$\{\varepsilon\} = [B]\{d\}, \tag{10}$$

where: $\{d\}$ – the vector of nodal displacement.

The FE formula consists in interpolating the displacements and moistures/temperatures in the element area by using the same interpolation functions. By equating the work performed by internal forces and by using the virtual work method, the equation (11) is obtained.

$$[K]\{\delta\} = \{P\} \tag{11}$$

where: $[K]$ – element stiffness matrix, $\{P\}$ – nodal load vector.

$$\{P\} = \iint [N]^T q \, dx \, dy \tag{12}$$

Equations (13-16) are used to determine the thermal load.

$$\{Pe^N\} = \iint [B]^T [H]^T \{F^N\} \, dx \, dy \tag{13}$$

$$\{F^N\}^T = \left[N_x^N, N_y^N, N_{xy}^N, M_x^N, M_y^N, M_{xy}^N, 0, 0, - - - \right] \tag{14}$$

$$\{N_x^N, N_y^N, N_{xy}^N\}^T = \sum_k^n \int_{z_{k-1}}^{z_k} \{\overline{Q}_{ij}\}_k \{\varepsilon\}_k \, dz \tag{15}$$

$$\{M_x^N, M_y^N, M_{xy}^N\}^T = \sum_k^n \int_{z_{k-1}}^{z_k} \{\overline{Q}_{ij}\}_k \{\varepsilon\}_k \tag{16}$$

where: $i, j = 1, 2, 6,$ $\{\varepsilon_k\}^T = [\varepsilon_x, \varepsilon_y, \varepsilon_{xy}].$

Without losing generality of the form, an arbitrary temperature distribution can be found as shown by equation (17).

$$T(x, y, z) = T_0 + \left(\frac{z}{h}\right) T_1(x, y), \tag{17}$$

where: T_0 – initial constant temperature.

Case No.1. Uniform temperature over the entire depth:

$$\begin{Bmatrix} \varepsilon_x \\ \varepsilon_y \\ \varepsilon_{xy} \end{Bmatrix} = \begin{Bmatrix} \alpha_x \\ \alpha_y \\ \alpha_{xy} \end{Bmatrix} \Delta T \tag{18}$$

$$\begin{Bmatrix} \alpha_x \\ \alpha_y \\ \alpha_{xy} \end{Bmatrix} = \begin{bmatrix} c^2 & s^2 & -2cs \\ s^2 & c^2 & 2cs \\ cs & -cs & c^2-s^2 \end{bmatrix} \left[Q \right]_k \begin{Bmatrix} \alpha_1 \\ \alpha_2 \\ \alpha_{12} \end{Bmatrix},$$

where: $\alpha_1, \alpha_2, \alpha_{12}$ – coefficients of thermal expansion referred to the main material axes of the laminate; $\alpha_x, \alpha_y, \alpha_{xy}$ – transformed coefficients of thermal expansion referred to the x-y coordinate system.

$$\{F\} = \oiiint \left[B \right]^T \left[H \right]^T \begin{Bmatrix} \alpha_x \\ \alpha_y \\ \alpha_{xy} \end{Bmatrix} T dv. \tag{19}$$

Case No. 2. Temperature varying over the entire depth:

$$\{F\} = \oiiint \left[B \right]^T \left[H \right]^T \begin{Bmatrix} \alpha_x \\ \alpha_y \\ \alpha_{xy} \end{Bmatrix} \left[\frac{1}{2} \left(T_U + T_L + \frac{z}{h} (T_U - T) \right) \right] T dv, \tag{20}$$

where: T_U – temperature on the upper surface; T_L – temperature on the lower surface.

3.1. Skew transformations

Due to the fact that the edges of boundary elements of skew shells are not parallel to the global axis, it is not possible to determine the boundary conditions in terms of global displacements u_0, w_0, v_0 etc. (Fig. 3).
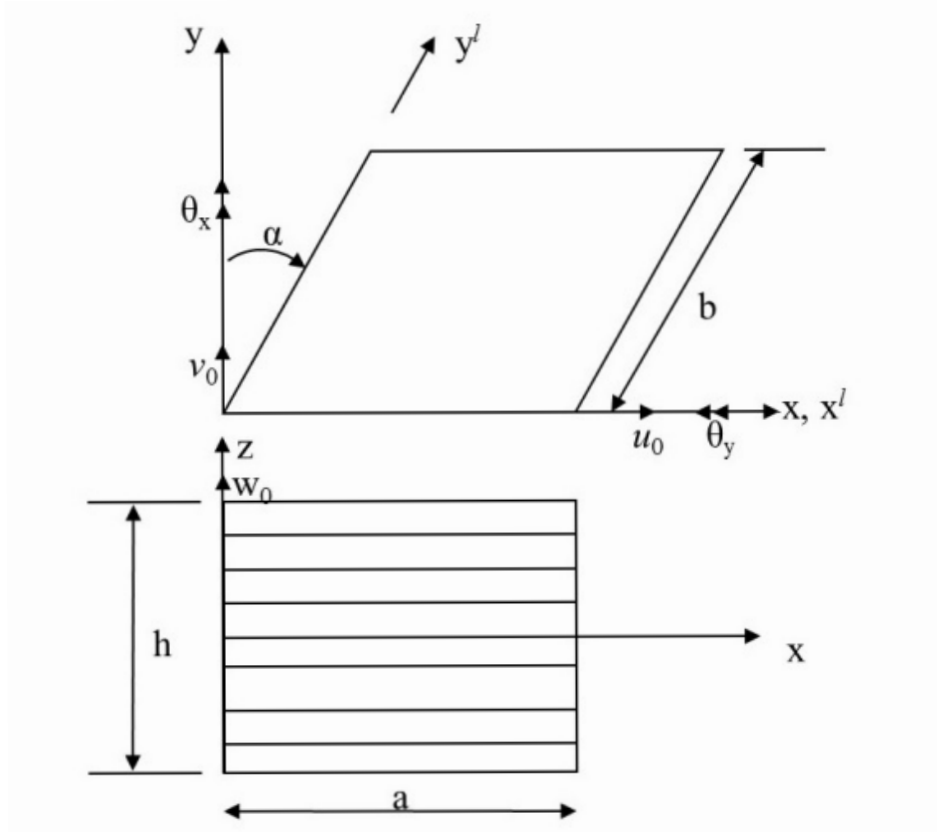
Fig. 3.   The geometry of skew laminated hyperbolic paraboloids. Source: own study

Therefore, in order to determine the necessary boundary conditions at the skew edge, edge displacements x^l, y^l, z^l in the local coordinates u_0^l, v_0^l, w_0^l should be used. For this purpose, the matrix of elements corresponding to the global axis shall be transformed into a local one [30] (21).

$$d_i = [\text{T}]d_i^l , \tag{21}$$

where: d_i^l, d_i – generalised displacement vectors in the local and global coordinate systems (22)(23).

$$\{d_i\} = \{u_0, v_0, w_0, \theta_x, \theta_y, \psi_x, \psi_y\}^T \tag{22}$$

$$\{d_i^l\} = \{u_0^l, v_0^l, w_0^l, \theta_x^l, \theta_y^l, \psi_x^l, \psi_y^l\}^T . \tag{23}$$

A nodal transformation matrix on the skew boundary is shown below.

$$
\text{Transformation matrix } [T] =
\begin{pmatrix}
\cos\alpha & -\sin\alpha & 0 & 0 & 0 & 0 & 0 \\
\sin\alpha & \cos\alpha & 0 & 0 & 0 & 0 & 0 \\
0 & 0 & 1 & 0 & 0 & 0 & 0 \\
0 & 0 & 0 & \cos\alpha & -\sin\alpha & 0 & 0 \\
0 & 0 & 0 & \sin\alpha & \cos\alpha & 0 & 0 \\
0 & 0 & 0 & 0 & 0 & \cos\alpha & -\sin\alpha \\
0 & 0 & 0 & 0 & 0 & \sin\alpha & \cos\alpha
\end{pmatrix},
\tag{24}
$$

4. Numerical problems

The following boundary conditions were used in the presented analysis:
a) Simply supported (SS):

$$\text{At } x = 0,\ a;\ v = w = \theta_y = \psi_y = 0 \tag{25}$$

$$\text{At } y = 0,\ b;\ u = w = \theta_x = \psi_x = 0 \tag{26}$$

b) Clamped (CC):

$$\text{At } x = 0,\ a \text{ and } y = 0,\ b;\ u = v = w = \theta_x = \theta_y = \psi_x = \psi_y = 0 \tag{27}$$

c) Clamped-simply supported (CS):

$$\text{At } x = 0 \text{ and } y = 0;\ u = v = w = \theta_x = \theta_y = \psi_x = \psi_y = 0 \tag{28}$$

$$\text{At } x = a;\ v = w = \theta_y = \psi_y = 0 \text{ and at } y = b;\ u = w = \theta_x = \psi_x = 0 \tag{29}$$

The non-dimensional formulae used in this paper are:

$$
\overline{w} = \frac{10wh}{\alpha_0 T_0 a^2},\quad
\overline{\sigma}_x = \left(\frac{a}{2},\frac{b}{2},-\frac{h}{2}\right)\frac{\sigma_x}{\alpha_0 T_0 E_T},\quad
\overline{\sigma}_y = \left(\frac{a}{2},\frac{b}{2},z\right)\frac{\sigma_y}{\alpha_0 T_0 E_T},\ \text{and}\ \
\overline{\tau}_{xy} = \left(0,0,-\frac{h}{2}\right)\frac{\tau_{xy}}{\alpha_0 T_0 E_T}.
\tag{30}
$$

The following material properties are used in this paper (unless otherwise stated): $\alpha_1/\alpha_2 = 3$, $\rho=1$, $\mu_{12}=0.25$, $E_1/E_2=25$, $G_{12}=G_{13}=0.5E_2$ and $G_{23}=0.2E_2$.

5. Results and discussion

5.1. Validation of the formula – a convergence study

As shown in Tab. 1, the convergence test was carried out by varying the mesh size from 12×12 to 20×20 (N_x and N_y – numbers of elements in x and y-direction).

Table 1. The convergence study of laminated (0°/90°) skew hyperbolic paraboloid (R_x/R_y = -0.5, skew angle = 15°) subjected to hygrothermal loading (ΔT = 1 and ΔC = 0.01%). Source: own study

Mesh Size	Non-dimensional deflection
12×12	2.4565
14×14	2.4505
16×16	2.4450
18×18	2.4449
20×20	2.4449

As shown in Tab. 1, the value of non-dimensional deflection converged for Nx×Ny = 16×16. Therefore, all subsequent analyses were carried out with the above-mentioned mesh size.

5.2. Validation of the formula – comparison of results

Tab. 2 shows the middle deflection (mm) of a two-ply (0°/90°) perpendicularly supported square laminate with different thickness ratios. The results are similar to those in [23]. The values of the middle deflection for rectangular SS laminated plates exposed to sinusoidal temperature gradient for (h/r) = 0.01 are shown in Tab. 3.

Table 2. In-plane and transverse displacements of double-layered (0°/90°) square laminate. Source: [23], own study

Thickness Ratio	Brischetto and Carrera [23]	Present
100	5.9448	5.9424
50	1.4857	1.4857
10	0.0587	0.0590
5	0.0141	0.0144

Table 3. Influence of the shape factor on the deflection in SS composite plates. Source: [16], [10], own study

Reference	0/90/0			0	0/90
	a/b=1	a/b=1.5	a/b=2	a/b=1	a/b=1
Present	1.0174	0.8585	0.6319	1.0226	1.1080
Singh and Chakrabarti [16]	1.0429	0.8802	0.6566	1.0332	1.1520
Reddy and Hsu [10]	1.0949	0.9847	0.7643	1.0313	1.6765

In order to validate the central transverse deflection of laminated shells subjected to sinusoidal temperature load of different curvature, these results were compared with the results of Khare et al. [24] and Brischetto [18] in Tab. 4. It can be seen in Tab. 4 that the current figures are similar to HSDT. Tab. 5 shows non-dimensional middle deflections of three-layer laminated rectangular plates (0°/90°/0°) subjected to sinusoidal hygrothermal distribution (ΔT = 300°C

and $\Delta C = 0.01\%$). Importantly, the current numerical result is in accordance with the results presented by Zenkour et al. [13].

Table 4.   Non-dimensional middle deflections of three-layer shells. Source: [24], [26], [18], own study

R/a	Present	Khare et al. [24] [HOST12]	Khare et al. [24] [FOST]	Khdeir et al. [26] [HSDT]	Brischetto [18]
Cylindrical shell (0/90) with a/b = 1, h/a = 0.1, $R_1 = \infty$, $R_2 = R$					
5	1.1249	1.1261	1.1272	1.1235	--
10	1.1423	1.1434	1.1444	1.1421	--
50	1.1481	1.1493	1.1501	1.1482	--
Spherical shell (0/90) with a/b = 1, h/a = 0.1, R1 = R2 = R					
5	1.0574	1.0588	1.0578	1.0545	--
10	1.1243	1.1256	1.1258	1.1235	--
50	1.1474	1.1487	1.1493	1.1475	--
Ten-layered cylindrical shell (0/90/…) with a/b = 1, h/a = 0.1, $R_1 = \infty$, $R_2 = R$					
5	1.0234	1.0224	1.0234	1.0216	1.0207
10	1.0308	1.0299	1.0307	1.0303	1.0283
50	1.0331	1.0325	1.0330	1.0332	1.0306

Table 5.   Non-dimensional middle deflections of three-layer (0°/90°/0°) laminates subjected to sinusoidal hygrothermal distribution. Source: [13], own study

a/b	a/h = 10		a/h = 20		a/h = 50	
	Present	Zenkour and Alghanmi [13]	Present	Zenkour and Alghanmi [13]	Present	Zenkour and Alghanmi [13]
1	2.7360	2.7749	2.1691	2.3654	1.9906	2.2355
1.5	3.2156	3.2273	2.9160	2.8521	2.8168	2.7148
2	3.0517	2.8496	2.9415	2.6631	2.8971	2.5849

5.3. Parametric study

Tab. 6 shows the dimensionless middle deflection of a three-layer hyperbolic paraboloid exposed to sinusoidal hygrothermal loading. The coefficient of curvature (R_x/R_y) was differentiated from -0.50 to -1.50. The value of dimensionless deflection increases as the curvature coefficient increases, and as the skew angle increases, the value of dimensionless deflection decreases.

Table 6.   Non-dimensional middle deflections of three-layer (0°/90°/0°) skew hyperbolic paraboloid subjected to sinusoidal hygrothermal distribution ($\Delta T = 300$ °C, $\Delta C = 0.01$%). Source: own study

Curvature	Skew angle	Boundary conditions		
		SS	CC	CS
-0.50	0^0	2.669	0.852	1.673
	15^0	2.445	0.809	1.480
	30^0	1.866	0.673	1.252
	45^0	1.137	0.444	1.016
	60^0	0.487	0.193	0.686
-0.10	0^0	2.741	1.243	1.768
	15^0	2.528	1.154	1.576
	30^0	1.953	0.904	1.260
	45^0	1.194	0.549	0.862
	60^0	0.509	0.219	0.450
-1.50	0^0	2.763	1.371	1.795
	15^0	2.553	1.267	1.604
	30^0	1.977	0.978	1.258
	45^0	1.210	0.582	0.806
	60^0	0.516	0.227	0.369

The dimensionless maximum deflection of skew hyperbolic paraboloids (with different lamination schemes) subjected to sinusoidal temperature and hygrothermal load are shown in Tab. 7. For a shell subjected to hygrothermal load, the value of maximum dimensionless deflection is greater than in a shell subjected to thermal load only. An angle-ply shell has less maximum dimensionless deflection than a cross-ply shell. As the skew angle increases, the dimensionless deflection decreases for the entire lamination scheme under consideration.

Table 7.   The non-dimensional central deflections of skew hyperbolic paraboloid under sinusoidal hygrothermal distribution ($\Delta T = 300$°C, $\Delta C = 0.01$%). Source: own study

Skew angle	$0°/90^0$	$45°/-45°$	$0°/90°/0°$	$45°/-45°/45°$	$0°/90°/90°/0°$
Temperature loading					
0^0	1.151	0.698	1.055	0.813	1.044
15^0	0.994	0.626	0.939	0.735	0.868
30^0	0.642	0.522	0.652	0.586	0.497
45^0	0.307	0.272	0.336	0.318	0.194
60^0	0.093	0.049	0.110	0.083	0.047
Hygrothermal loading					
0^0	6.805	2.728	2.741	2.313	2.559
15^0	5.914	3.113	2.528	2.315	2.118
30^0	3.893	3.017	1.953	1.950	1.173
45^0	1.924	1.857	1.194	1.179	0.426
60^0	0.633	0.578	0.509	0.385	0.089

Tab. 8 shows dimensionless middle deflections of laminated hyperbolic paraboloids of varying thickness. The maximum dimensionless deflection is noticeable for the shell for which a/h = 5, and when thickness decreases, the dimensionless deflection increases to a/h = 50. Tabs 9-10 show the change of material properties with the change in temperature and moisture content. The maximum deflection of laminated hyperbolic paraboloids subjected to

different thermal loads is shown in Tab. 11. The deflection of the shell was found to increase as the temperature rises. Tab. 12 shows the maximum deflection of hyperbolic paraboloids with different moisture concentrations in the laminate layer. The value of dimensionless deflection increases as moisture concentration increases. Tabs 13-15 show non-dimensional stresses ($\bar{\sigma}_x$, $\bar{\sigma}_y$ and $\bar{\tau}_{xy}$) of a laminated rhombic hyperbolic paraboloid subjected to hygrothermal loading (in the same location as above). The maximum stresses are observed to depend on the skew angle and boundary conditions.

Table 8. The non-dimensional central deflections of a laminated skew hyperbolic paraboloid under sinusoidal hygrothermal loading. Source: own study

Skew angle	a/h = 5	a/h = 10	a/h = 20	a/h = 50	a/h = 100
SS					
0^0	6.650	6.805	6.852	6.870	6.860
15^0	5.831	5.914	5.896	5.814	5.496
30^0	3.883	3.893	3.832	3.673	3.164
45^0	1.880	1.924	1.906	1.805	1.494
60^0	0.577	0.633	0.648	0.619	0.528
CC					
0^0	1.921	1.956	1.887	1.336	0.696
15^0	1.692	1.757	1.720	1.256	0.671
30^0	1.127	1.233	1.262	1.013	0.592
45^0	0.529	0.618	0.674	0.625	0.438
60^0	0.153	0.188	0.219	0.230	0.207

Table 9. Material properties at moisture concentrations $G_{13} = G_{12}$, $G_{23} = 0.5\ G_{12}$, $\nu_{12}=0.3$, $\beta_1 = 0$, and $\beta_2 = 0.44$. Source: own study

Elastic moduli	Moisture concentration (C %)						
	0	0.25	0.5	0.75	1.0	1.25	1.5
E_1	130	130	130	130	130	130	130
E_2	9.5	9.25	9.0	8.75	8.5	8.5	8.5
G_{12}	6.0	6.0	6.0	6.0	6.0	6.0	6.0

Table 10. Material properties at various temperatures ($G_{13} = G_{12}$, $G_{23} = 0.5\ G_{12}$, $\nu_{12} = 0.3$, $\alpha_1 = -0.3 \times 10^{-6}$, and $\alpha_2 = 28.1 \times 10^{-6}$). Source: own study

Elastic moduli	Temperature T(K)					
	300	325	350	375	400	425
E_1	130	130	130	130	130	130
E_2	9.5	8.5	8.0	7.5	7.0	6.75
G_{12}	6.0	6.0	5.5	5.0	4.75	4.5

Table 11. Maximum deflection of laminated skew hyperbolic paraboloids under various temperature loading. Source*: own study*

Skew angle	$\Delta T = 300$	$\Delta T = 325$	$\Delta T = 350$	$\Delta T = 375$	$\Delta T = 400$	$\Delta T = 425$
SS						
0°	1.582	1.592	1.685	1.770	1.823	1.912
15°	1.382	1.391	1.470	1.543	1.588	1.665
30°	0.925	0.932	0.983	1.028	1.057	1.107
45°	0.470	0.475	0.499	0.520	0.533	0.557
60°	0.161	0.163	0.170	0.176	0.181	0.188
CC						
0°	0.510	0.517	0.541	0.561	0.575	0.600
15°	0.458	0.464	0.486	0.504	0.517	0.539
30°	0.323	0.327	0.342	0.355	0.364	0.379
45°	0.164	0.167	0.174	0.180	0.184	0.191
60°	0.051	0.052	0.053	0.055	0.056	0.058

Table 12. Maximum deflection of laminated skew hyperbolic paraboloids with different moisture concentrations. Source*: own study*

Skew angle	Moisture Concentration (C %)					
	0.25	0.5	0.75	1.0	1.25	1.5
0°	0.312	0.613	0.903	1.181	1.560	1.872
15°	0.303	0.596	0.878	1.149	1.516	1.819
30°	0.268	0.527	0.776	1.017	1.339	1.607
45°	0.194	0.382	0.564	0.739	0.971	1.166
60°	0.099	0.196	0.289	0.379	0.496	0.596

Table 13. Non-dimensional stress ($\bar{\tau}_{xy}$) of laminated skew hyperbolic paraboloids with different boundary conditions. Source*: own study*

Skew angle	SS	CC	CS
0°	0.393	0.000	0.000
15°	0.730	0.000	0.000
30°	0.720	0.000	0.000
45°	0.327	0.000	0.000
60°	-0.165	0.000	0.000

Table 14. Non-dimensional in-plane stress ($\bar{\sigma}_x$) of laminated skew hyperbolic paraboloids with different boundary conditions. Source*: own study*

Skew angle	SS	CC	CS
0°	-10.683	-3.982	2.098
15°	-15.822	-11.624	-5.501
30°	-15.410	-18.386	-12.456
45°	-8.098	-23.419	-13.686
60°	2.064	-25.237	-7.833

Table 15. Non-dimensional in-plane stress ($\bar{\sigma}_y$) of laminated skew hyperbolic paraboloids with different boundary conditions. Source: own study

Skew angle	SS	CC	CS
0°	0.480	0.019	0.250
15°	0.300	-0.151	0.201
30°	0.036	-0.416	0.005
45°	0.637	0.791	0.781
60°	4.664	8.041	4.906

6. Conclusions

A C^0 finite element (FE) formulation was developed using Sanders' approximations and was applied to study the static reaction of a composite skew hyperbolic paraboloid exposed to hygrothermal loading. Many new results were obtained concerning the hygrothermal reaction of laminated hyperbolic paraboloids with different moisture concentration, thickness ratio, skew angle, boundary conditions, radius of curvature, temperature and layer orientation, which should be beneficial for future studies.

General conclusions are as follows:

- As the curvature coefficient increases, the value of dimensionless deflection increases.
- As the skew angle increases, the dimensionless deflection decreases.
- The dimensionless deflection increases as the moisture concentration increases.
- An angle-ply shell shows less maximum non-dimensional deflection than a cross-ply shell.
- The deflection of the shell increases as the temperature changes.
- In a shell subjected to hygrothermal load, the maximum value of non-dimensional deflection is greater than in a shell subjected to thermal load only.

References

[1] Suchorab, Z., Sobczuk, H., Łagód, G., "Estimation of building material moisture using non-invasive TDR sensors", in Thermophysics 2016: 21st International Meeting. AIP Conference Proceedings, vol. 1752, 2016, pp. 1–7. https://doi.org/10.1063/1.4955231

[2] Suchorab, Z. et al., "A Noninvasive TDR Sensor to Measure the Moisture Content of Rigid Porous Materials", *Sensors (Basel),* vol. 11(18): 3935, (2018), pp. 1-20. https://doi.org/10.3390/s18113935

[3] Barnat-Hunek, D., Siddique, R., Łagód, G., "Properties of hydrophobised lightweight mortars with expanded cork", *Construction and Building Materials,* vol. 155, (2017) pp. 15–25. https://doi.org/10.1016/j.conbuildmat.2017.08.052

[4] Pipes, R.B., Vinson, J.R., Chou, T.W., "On the Hygrothermal Response of Laminated Composite Systems", *Journal of Composite Materials,* vol. 10 (1976), pp. 129–148. https://doi.org/10.1177/002199837601000203

[5] Wu, C.H. and Tauchert, T.R., "Thermoelastic analysts of laminated plates. 2: Antisymmetric cross-ply and angle-ply laminates", *Journal of Thermal Stresses,* vol. 3, (1980), pp. 365–378. https://doi.org/10.1080/01495738008926975

[6] Lee, S.Y. and Yen, W.J., "Hygrothermal effects on the stability of a cylindrical composite shell panel", *Computers & Structures*, vol. 33, (1989), pp. 551–559. https://doi.org/10.1016/0045-7949(89)90029-1

[7]   Whitney, J.M. and Ashton, J.E., "Effect of environment on the elastic response of layered composite plates", *American Institute of Aeronautics and Astronautics Journal,* vol. 9(9), (1971), pp. 1708–1713. https://doi.org/10.2514/3.49976

[8]   Pell, W.H., "Thermal deflections of anisotropic thin plates", *Quarterly Applied Mathematics,* vol. 4, (1940), pp. 27–44. https://doi.org/10.1090/qam/16032

[9]   Sai Ram, K.S. and Sinha, P.K., "Hygrothermal effects on the bending characteristics of laminated composite plates", *Computers & Structures,* vol. 40, (1991), pp. 1009–1015. https://doi.org/10.1016/0045-7949(91)90332-G

[10] Reddy, J.N. and Hsu, Y.S., "Effects of shear deformation and anisotropy on the thermal bending of layered composite plates", *Journal of Thermal Stresses*, vol. 3, (1980), pp. 475–493. https://doi.org/10.1080/01495738008926984

[11] Doxsee, L.E., "A higher-order theory of hygrothermal behavior of laminated composite shells", *International Journal of Solids and Structures*, vol. 25, (1989), pp. 339–355. https://doi.org/10.1016/0020-7683(89)90052-8

[12] Lee, S.Y. et al., "Hygrothermal effects on the linear and nonlinear analysis of symmetric angle-ply laminated plates", *Composite Structures*, vol. 21, (1992), pp. 41–48. https://doi.org/10.1016/0263-8223(92)90078-Q

[13] Zenkour, A.M. and Alghanmi, R.A., "Bending of symmetric cross-ply multilayered plates in hygrothermal environments", *Journal of Mathematical Models in Engineering*, vol. 2, (2016), pp. 94–107. https://doi.org/10.21595/mme.2016.17405

[14] Biswal, M., Sahu, S.K., Asha, A. V., "Experimental and numerical studies on free vibration of laminated composite shallow shells in hygrothermal environment", *Composite Structures*, vol. 127, (2015), pp. 165–174. https://doi.org/10.1016/j.compstruct.2015.03.007

[15] Zenkour, A.M. and Fares, M.E., "Thermal bending analysis of composite laminated cylindrical shells using a refined first-order theory", *Journal of Thermal Stresses*, vol. 23, (2000), pp. 505–526, https://doi.org/10.1080/014957300403969

[16] Singh, S.K. and Chakrabarti, A., "Hygrothermal analysis of laminated composite plates by using efficient higher order shear deformation theory", *Journal of Solid Mechanics*, vol. 3, (2011), pp. 85–95.

[17] Zenkour, A.M., "Analytical solution for bending of cross-ply laminated plates under thermo-mechanical loading", *Composite Structures*, vol. 65, (2004), pp. 367–379. https://doi.org/10.1016/j.compstruct.2003.11.012

[18] Brischetto, S., "Hygrothermoelastic analysis of multilayered composite and sandwich shells", *Journal of Sandwich Structures & Materials*, vol. 15, (2013), pp. 168–202. https://doi.org/10.1177/1099636212471358

[19] Upadhyay, A.K., Pandey, R., Shukla, K.K., "Nonlinear flexural response of laminated composite plates under hygro-thermo-mechanical loading", *Communications in Nonlinear Science and Numerical Simulation*, vol. 15, (2010), pp. 2634–2650. https://doi.org/10.1016/j.cnsns.2009.08.026

[20] Ali, J.S.M., Alsubari, S., Aminanda, Y., "A Higher Order Theory for Bending of Cross Ply Laminated Cylindrical Shell under Hygrothermal Loads", *Advanced Materials Research*, vol. 1115, (2015), pp. 509–512. https://doi.org/10.4028/www.scientific.net/amr.1115.509

[21] Patel, B.P., Ganapathi, M., Makhecha, D.P., "Hygrothermal effects on the structural behaviour of thick composite laminates using higher-order theory", *Composite Structures*, vol. 56, (2002), pp. 25–34. https://doi.org/10.1016/S0263-8223(01)00182-9

[22] Ali, J.S.M., Bhaskar, K., Varadan, T.K., "A new theory for accurate thermal/mechanical flexural analysis of symmetric laminated plates", *Composite Structures*, vol. 45, (1999), pp. 227–232. https://doi.org/10.1016/S0263-8223(99)00028-8

[23] Brischetto, S. and Carrera, E., "Coupled thermo-mechanical analysis of one-layered and multi-layered isotropic and composite shells", *CMES: Computer Modeling in Engineering & Sciences*, vol. 56(3), (2010), pp. 249–302. https://doi.org/10.3970/cmes.2010.056.249

[24] Khare, R.K., Kant, T., Garg, A.K., "Closed-form thermo-mechanical solutions of higher-order theories of cross-ply laminated shallow shells", *Composite Structures*, vol. 59, (2003), pp. 313–340. https://doi.org/10.1016/S0263-8223(02)00245-3

[25] Tauchert, T.R., "Thermally induced flexure, buckling, and vibration of plates", *Applied Mechanics Reviews*, vol. 44, (1991), pp. 347–360. https://doi.org/10.1115/1.3119508

[26] Khdeir, A.A., Rajab, M.D., Reddy, J.N., "Thermal effects on the response of cross-ply laminated shallow shells", *International Journal of Solids and Structures*, vol. 29, (1992), pp. 653–667. https://doi.org/10.1016/0020-7683(92)90059-3

[27] Jin, Q. and Yao, W., "Hygrothermal analysis of laminated composite plates in terms of an improved C0-type global–local model", *Aerospace Science and Technology*, vol. 63, (2017), pp. 328–343. https://doi.org/10.1016/j.ast.2017.01.004

[28] Lal, A.; Singh, B.N., Anand, S., "Nonlinear bending response of laminated composite spherical shell panel with system randomness subjected to hygro-thermo-mechanical loading", *International Journal of Mechanical Sciences*, vol. 53, (2011), pp. 855–866. https://doi.org/10.1016/j.ijmecsci.2011.07.008

[29] Chao, W.C. and Reddy, J.N., "Analysis of laminated composite shells using a degenerated 3-D element", *International Journal for Numerical Methods in Engineering*, vol. 20, (1984), pp. 1991–2007. https://doi.org/10.1002/nme.1620201104

[30] Ali, J.S.M., Alsubari, S., Aminanda, Y., "Hygrothermoelastic analysis of orthotropic cylindrical shells", *Latin American Journal Solids Structures*, vol. 13, (2016), pp. 573–589. https://doi.org/10.1590/1679-78252249